Pergamon

0301-9322(93)E0011-S

*Int. J. Multiphase Flow* Vol. 20, No. 2, pp. 315–338, 1994
Copyright © 1994 Elsevier Science Ltd
Printed in Great Britain. All rights reserved
0301-9322/94 $7.00 + 0.00

# MODELING OF SOLIDS GLOBAL FLUCTUATIONS IN BUBBLING FLUIDIZED BEDS BY STANDING SURFACE WAVES

J. G. SUN,[1] M. M. CHEN[2] and B. T. CHAO[2]

[1]Argonne National Laboratory, 9700 South Cass Ave, Argonne, IL 60439, U.S.A.

[2]Department of Mechanical and Industrial Engineering, University of Illinois at Urbana-Champaign, 1206 West Green St, Urbana, IL 61801, U.S.A.

*(Received 10 July 1991; in revised form 19 October 1993)*

**Abstract**—The characteristics of solids global fluctuation in gas fluidized beds was examined. It was identified that sloshing is a dominant mechanism in bubbling fluidized beds. Experiments were conducted using the computer-aided particle tracking facility to examine the solids sloshing motions and to determine the fluctuation frequency. For cylindrical beds of intermediate depths, there are two modes of sloshing; namely, the axisymmetric mode and the antisymmetric mode. A standing surface wave model has been developed to predict the global fluctuation frequency of the solids sloshings in beds of intermediate and shallow depth. The axisymmetric and the antisymmetric modes of sloshing in cylindrical beds are the full- and half-wave modes of the standing surface waves. The model predictions for the sloshing frequency were found to be in good agreement with the experimental data of this study and with others in the literature. More importantly, it was found that, although the excitation for bed fluctuations originates from bubbles, the fluctuation frequency is controlled by surface waves.

*Key Words:* frequency prediction, solids global fluctuation, standing surface wave

## 1. INTRODUCTION

Solids motion in a gas fluidized bed is characterized by fluctuations. Depending on the experimental conditions, such as particle material and morphology, bed geometry, gas velocity etc., the fluctuations may be associated with bubbling, slugging, turbulence or their combination. Bubbling and slugging occur at gas velocities which are low compared with the particle's terminal velocity and the fluctuations have dominant characteristic frequencies. This paper focuses on bubbling beds only.

Pressure measurement using sensitive transducers located on the walls of a fluidized bed at various axial locations has been the common technique used to study solids fluctuations. The pressure fluctuation and the concomitant solids fluctuating motion are induced by the bubbles or slugs rising in the bed and bursting on the bed surface (Tamarin 1964; Hiby 1967; Lirag & Littman 1971; Fan *et al.* 1981). In shallow gas fluidized beds, harmonic pressure oscillations about their equilibrium states have been observed (Hiby 1967; Verloop & Heertjes 1974). As the bed height increases, the fluctuations become less regular and deviate from being harmonic. In the upper portion of the bed, it is the motion of the large bubbles that dominates the behavior of the pressure fluctuations. In the lower portion of the bed, pressure fluctuations are associated not only with the large bubbles in the central region of the bed formed through bubble coalescence, but also smaller bubbles that exist above the gas distributor plate. The latter are responsible for pressure fluctuations of smaller amplitude but higher frequencies (Fan *et al.* 1981). For beds of small diameter and large depth, bubble coalescence is complete in a major fraction of the column, resulting in the formation of slugs, and distinctly coherent pressure fluctuations can be observed (Baeyens & Geldart 1974; Svoboda *et al.* 1984; Noordergraaf *et al.* 1987).

The origin of solids fluctuations in fluidized beds has been examined by Jackson (1963), Anderson & Jackson (1968), Homsy *et al.* (1980) and Didwania & Homsy (1981a) using linear instability analysis based on the two-phase equations of fluidization. These studies showed that the state of uniform fluidization is unstable to small perturbations of voidage. In liquid fluidized beds, the growth rate is low and the development of the porosity waves could be observed experimentally

(Anderson & Jackson 1969; El-Kaissy & Homsy 1976). In gas fluidized beds, however, the predicted rate of growth of instability is so rapid that it can hardly be observed from experiments (Anderson & Jackson 1968). Although statements have been made that the growth of the small voidage disturbances would result in the formation of bubbles, the linear analyses just cited can only provide information on the initial state of the bed fluctuations.

Hiby (1967) considered the spontaneous vertical oscillation of individual particles in shallow fluidized beds. He first calculated the resonance frequency of a particle that was bound to its mean position resulting from the combined action of gravity and the quasi-elastic lifting force due to fluid flow. The oscillation frequency of the entire bed was then taken to be the weighted mean of the natural frequencies of the different layers of the particles. This model was later modified by Verloop & Heertjes (1974) by assuming that all particles in the bed oscillate in phase and of same frequency. For a shallow bed, the frequency is

$$f = \frac{1}{2\pi}\left[\frac{g}{H}\left(\frac{2-\epsilon}{\epsilon}\right)\right]^{1/2}. \qquad [1]$$

The foregoing relationship holds when the bed height is less than a critical value, which occurs when the porosity wave reaches the bed surface in half period. Beyond this critical height, slugging occurs and the oscillation frequency can then be related to the bubble rise velocity. It is given by

$$f_s = 0.35\frac{(gD)^{1/2}}{H_{mf}}. \qquad [2]$$

Jones & Pyle (1971) and Goossens (1976) used a similar approach and their results generally agree with those of Hiby (1967) and of Verloop & Heertjes (1974).

Davidson (1968) examined the influence of the compressibility of the gas in the plenum beneath the bed when the resistance of the distributor was low. He assumed that the solids in the bed behaved like an oscillating solid mass, compressing and rarifying the gas in the plenum. This model was commonly referred to as the piston model and for an undamped system the natural frequency is

$$f = \frac{1}{2\pi}\left(\frac{\gamma PA^2}{MV}\right)^{1/2}. \qquad [3]$$

Wong & Baird (1971) modified the model by including the effect of the permeability of the particulate phase, which acts like a damper for the pressure fluctuation. The predicted fluctuation frequency is generally smaller than that of [3].

Baeyens & Geldart (1974) developed a model for the pressure fluctuation in slugging fluidized beds. The frequency of the solids fluctuation was evaluated from the slug velocity and the distance between the consecutive slugs. It is given by

$$f_s = \frac{0.35}{k}\left(\frac{g}{D}\right)^{1/2}, \qquad [4]$$

where $k$ is a parameter depending on the bed diameter and height. For very deep beds with complete bubble coalescence, their experimental data showed that $k$ depends only on the bed diameter and $k = 9.38D^{-0.357}$ ($D$ in cm). It should be noted that the dependence of $f_s$ on $D$ is different from that in [2].

More recently, Fan *et al.* (1984) and Hiraoka *et al.* (1984) proposed a dynamic model based on the conjecture that the solids fluctuations consisted of the present fluctuations due to the flow of bubbles in the bed and the time-delayed fluctuations of the gas flow through the distributor. An integral dynamic equation relating the bed height to the various physical parameters was derived. The equation was then linearized for small fluctuations of the various quantities, and the solution of the linearized equation provided the dominant frequency. The model predicted a discontinuous change in the frequency at certain bed heights, which, as they claimed, could be observed from experimental results of Verloop & Heertjes (1974). The resulting relationship between the dominant frequency and the bed parameters is very complicated.

From this brief literature review, it was seen that implicit in all models was that the solids at any horizontal level oscillated in phase along the vertical bed column like plane waves. Accordingly, they are strictly applicable to slugging fluidized beds. Although attempts were made to correlate data obtained in bubbling beds, they had not been successful. For instance, Baeyens & Geldart (1974) reported that for beds with $H/D$ less than about 2 (identified as bubbling beds in their analysis) the measured frequencies could not be interpreted by their slugging model and, therefore, the data were not presented. Svoboda *et al.* (1983, 1984) and Rockey *et al.* (1989) found that the dominant bed frequency would increase or decrease with the fluidizing gas velocity, depending on the experimental conditions. Such observations could not be explained by the slugging models. In this study we propose that there is another mechanism of solids fluctuations which is induced by bubble disturbance. The fluctuations are the results of axisymmetric and antisymmetric solids sloshings and are dominant in bubbling fluidized beds. Experiments were conducted using the computer-aided particle tracking facility (CAPTF) to examine these modes of fluctuations and to determine their frequencies. A standing surface wave model was proposed for their prediction.

## 2. COMPUTER-AIDED PARTICLE TRACKING FACILITY (CAPTF)

A description of the principle of operation of the CAPTF and its associated data acquisition and processing schemes has been documented previously (Lin 1981; Liljegren 1983; Lin *et al.* 1985; Moslemian 1987). It can be operated in the single- or swarm-particle tracking mode. In the single-particle tracking mode, a radioactive tracer, dynamically identical to the bed particles under study, is introduced into the fluidized bed and its instantaneous position is tracked by an array of 16 scintillation detectors. Details of its use for the determination of the instantaneous Lagrangian velocity of the tracer can be found in the four references just cited. The swarm-particle tracking mode was used in the present investigation to study solids fluctuations. In this mode, a small amount (typically 10 g) of radioactive particles were used as tracers. In the present experiments, they were simply the bed particles (soda-lime glass beads), activated in a nuclear reactor to convert the sodium in the glass to its radioactive isotope $^{24}Na$ which has a half-life of about 15 h. Following the introduction of the tracers into the bed, their subsequent migration and dispersion were monitored by the 16 scintillation detectors surrounding the bed as illustrated in figure 1. The detectors were arranged in 4 levels, located at 540, 382, 218 and 54 mm above the distributor plate. At each level, there were 4 detectors, 90° apart in a horizontal plane. They were also staggered

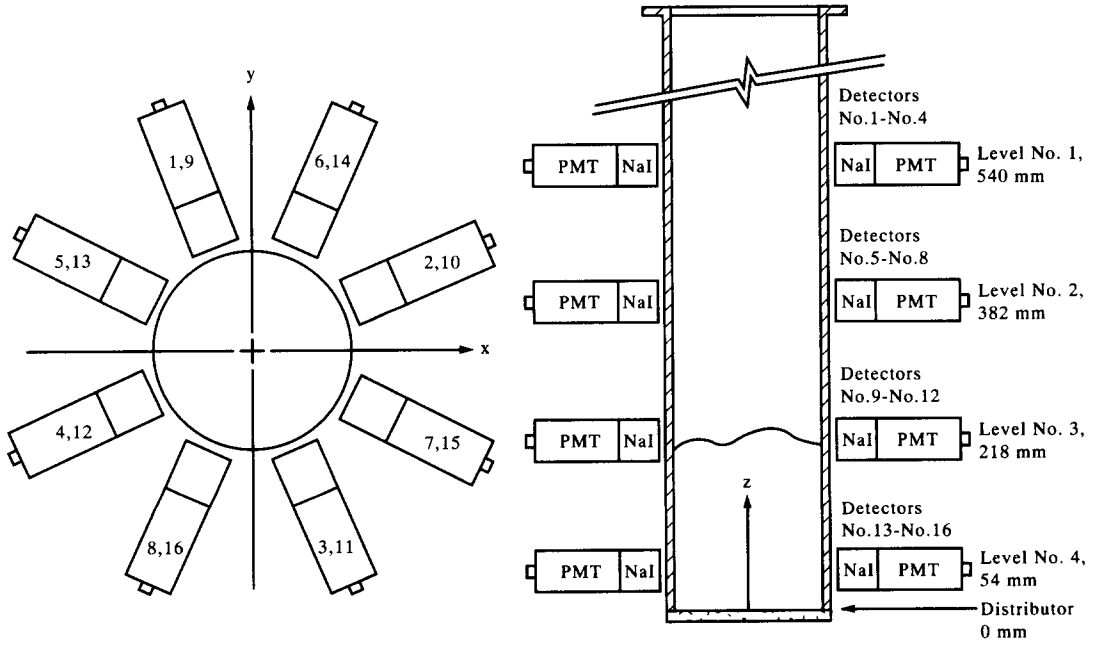


Figure 1. Arrangement of detectors around a cylindrical bed.

vertically. The arrangement was designed primarily for particle velocity measurements using the single-particle tracking mode. In the present investigation, only detectors in level 3, Nos 9–12, were relevant since they were approximately at the same level as the free surface of the bubbling bed. After the initial transients, the detector signals (count rates) settled down to statistically stationary values representing the uniformly mixed condition. The transient portion of the detector signals is related to the mixing rate (Moslemian 1987), and the time variations of the signals in the statistically stationary state provide the desired information on the fluctuating frequency of the bulk solids motion.

## 3. MEASUREMENT OF THE SOLIDS GLOBAL FLUCTUATION FREQUENCY

The fluidized bed used in this study was constructed from a plexiglass tube of 190.5 mm (7.5 in.) inside diameter. The air distributor was made of sintered plastic plate with a nominal pore size of 90 $\mu$m. The bed particles were soda-lime glass spheres of diameters ranging from 425 to 600 $\mu$m with a mean of 500 $\mu$m and diameters from 600 to 850 $\mu$m with a mean of 705 $\mu$m. They have a specific gravity of 2.50 g/cm$^3$. These glass spheres are class B particles according to Geldart's (1973) classification. They are characterized by the formation of bubbles at or near the minimum fluidization velocity, $u_{mf}$, which was determined experimentally by the usual pressure drop method. It was found that $u_{mf} = 21.9$ and 30.2 cm/s for the 500 and 705 $\mu$m particles, respectively.

Experiments were performed for the 500 $\mu$m particles at $u_0/u_{mf} = 1.5$, 2, 3, 4 and 6 ($\mu_{mf} = 21.9$ cm/s) and for the 705 $\mu$m particles at $u_0/u_{mf} = 1.5$, 2, 3, 4 and 5 ($u_{mf} = 30.2$ cm/s), $u_0$ being the superficial fluidization velocity. The static bed height was set at 190 mm in all the experiments. Three sets of data were collected for each operating condition, and for each set 512 discrete signals were recorded by each detector at 30 ms intervals, giving a record length of 15.36 s. As we shall soon demonstrate, the frequency at which the data were acquired satisfied the Nyquist criterion.

### *3.1. Behavior of Solids Global Fluctuations*

From the visual observation of the fluidized bed in operation, at least two distinct modes of fluctuations have been noticed; namely, an axisymmetric mode and an antisymmetric mode of the solids sloshing motion. The existence of the two modes can be identified by examining the signals of the diametrically opposite detector pairs, 9–11 and 10–12 in level 3. The signals from detectors 9 and 11 are reproduced in figure 2 for the 500 $\mu$m particles at $u_0/u_{mf} = 2$. It is seen that most of the time the fluctuations are in phase, indicating the presence of axisymmetric oscillations. Occasionally, however, out-of-phase fluctuations are also found (between time periods 4.5–5.4 s and 7.2–8.1 s in figure 2), indicating the presence of antisymmetric sloshing motions. In passing, we note that only when the vertical plane along which the antisymmetric sloshing occurred was parallel to the axis of detectors Nos 9 and 11, are the out-of-phase fluctuations revealed in the figure. When the antisymmetric sloshing was perpendicular to the detector axis, the out-of-phase fluctuations were not revealed. The latter, however, can be seen from the signals of the detector pair 10–12. As it turned out, for the operating conditions used in the present investigation, the antisymmetric sloshing was dominant.

### *3.2. Interpretation of Detector Signals*

The response of a scintillation detector to $\gamma$-radiation from a group of radioactive particles depends on (1) the solid angle subtended by the group of particles at the center of the detector crystal and (2) the intervening mass attenuation. In general, the closer the group of particles is to the detector, the greater is its output and the higher is the measurement sensitivity. In the swarm-particle tracking mode, the tracers, subsequent to initial transients, are essentially uniformly mixed with the bed particles. Accordingly, the distribution of the sources of radiation and that of the bed density are the same. Hence, associated with detectors in a given level, there exists the "most sensitive volume" of particles where radiation has a characteristic influence on the detector output. From the signals shown in figure 2, the mean count rate and the mean peak-to-peak count rate variation can be determined and the results are given in table 1. Included in table 1 are similar results for detectors at three other levels. The mean count rate recorded by detectors in level 1 is

Table 1. Measured and calculated count rates and their variations

| Level | Mean count rate | P–P count rate variation (%) |
|---|---|---|
| 1 | 225 | 28 |
| 2 | 590 | 24 |
| 3 | 1650 | 25 |
| 4 | 2050 | 13 |

the lowest and that in level 4 is the highest, as one would expect from simply the solid angle consideration. The mean peak-to-peak count rate variations, expressed as a percentage of the mean, for detectors in levels 1, 2 and 3 are approximately the same since their associated "most sensitive volumes" are all adjacent to the free surface through which bubbles emerge and burst. These detectors see for a portion of time more air with sparsely distributed particles than in another portion of time, resulting in count rate fluctuations. On the other hand, the "most sensitive volume" associated with detectors in level 4 is bounded by the air distributor plate at its bottom and by the cylindrical wall of the bed on its side, and the count rate fluctuation is mainly due to the rising bubbles in the vicinity of the distributor plate. In the present investigation, our primary interest is the mode and frequency of the global motion of the particles near the free surface. Hence, the output of the detectors in level 3 is the most relevant, provided that its associated "most sensitive volume" has a length scale comparable to the radius of the cylindrical bed.

The mean peak-to-peak count rate fluctuation of detectors in level 3 is 25% of its mean (see table 1). An estimate of the extent of the "most sensitive volume" can be made by defining it to be such that 25% of the radiation seen by its scintillation crystal originates from that volume. The results obtained by ignoring attenuation are shown in figure 3 for detectors in levels 1, 2 and 3. It is seen that the length scale of the "most sensitive volume" associated with detectors at level 3 is approximately 1/3 of the diameter of the cylindrical bed. Had one chosen a different definition for the "most sensitive volume", say 50% of the total count rate, the length scale would be larger but not by a significant amount. It is therefore concluded that the *mode* (sloshing vs slugging) and the *frequency* of the global motion of particles in the free surface region are reflected in the outputs of detectors in level 3.

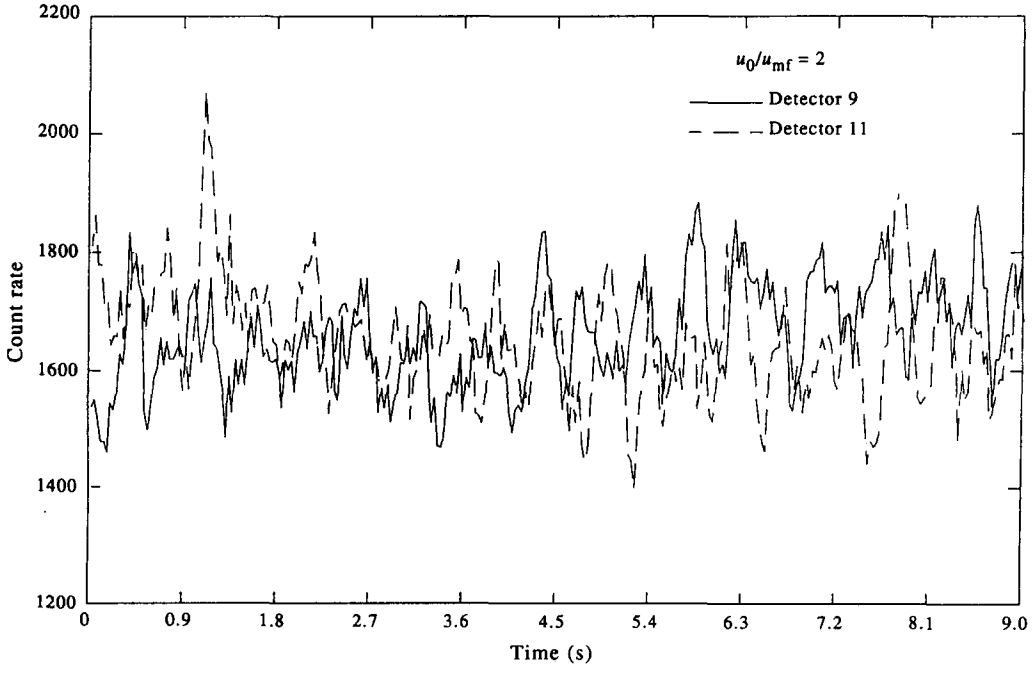


Figure 2. Variation of count rates from two diametrically opposite detectors, 500 $\mu$m glass particles at $u_0/u_{mf} = 2(u_{mf} = 21.9$ cm/s).

### *3.3. Statistical Properties of the Fluctuations*

To extract the mode, frequency and other information from the detector signals described in section 3.1, we examine their cross-correlations, autocorrelations and power spectral density (PSD) functions. For discrete detector signals of zero mean acquired at a sampling time interval $\delta t_s$, $x_n = x(n\delta t_s)$ and $y_n = y(n\delta t_s)$, $n = 1, 2, \ldots, N$, $N$ being the length of one set of signals, the cross-correlation function, $C_{xy}$, can be evaluated from (Bendat & Piersol 1986):

$$C_{xy}(r\delta t_s) = \frac{1}{N-r}\sum_{n=1}^{N-r} x_n y_{n+r}, \quad r = 0, 1, \ldots, m, \qquad [5]$$

where $r$ is the lag number and $m$ is the maximum lag number ($m < N$). The autocorrelation function, $C_{xx}$, can also be evaluated from [5] by simply replacing $y$ by $x$. The PSD function is determined directly from the Fourier transform of the signal. Using a Hamming window function to reduce the power leakage to side lobes in the frequency domain, the discrete Fourier transform of the signal $x_n$ is

$$X(f_k) = \delta t_s \sqrt{\frac{8}{3}} \sum_{n=1}^{N-1} x_n \left[1 - \cos^2\left(\frac{\pi n}{N}\right)\right] \exp\left(-\frac{i2\pi kn}{N}\right), \quad k = 1, 2, \ldots, N-1, \qquad [6]$$

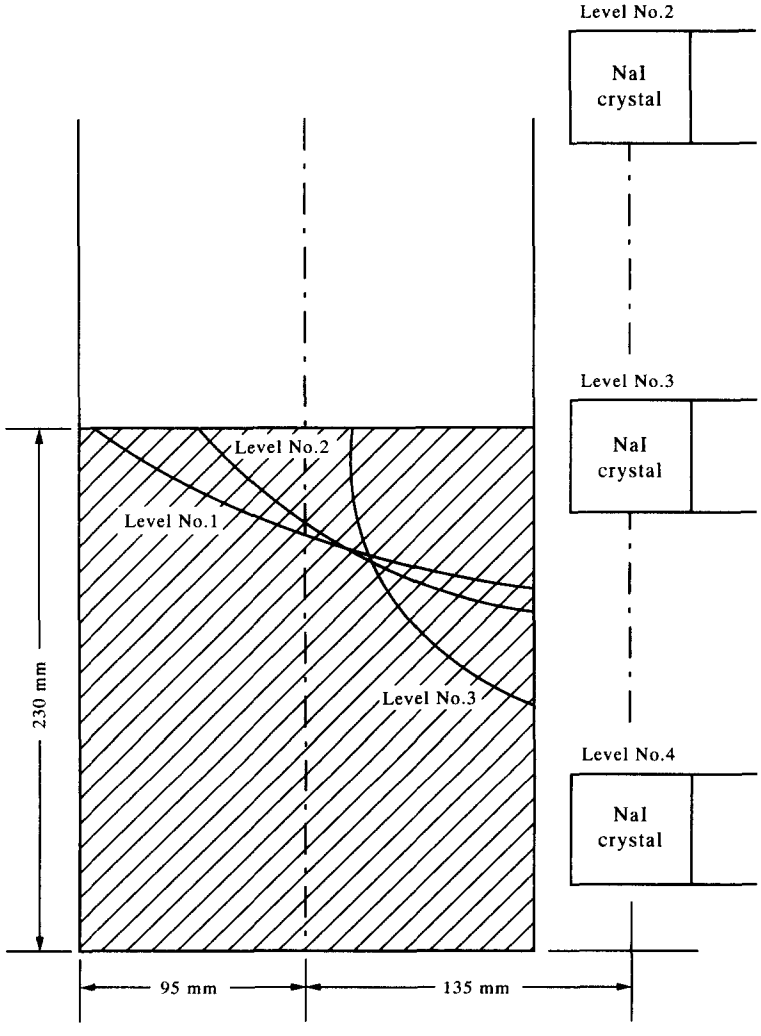


Figure 3. Volumes contributing 25% of the total count rates for detectors at the three levels. Each volume is a portion of a sphere centered at the NaI crystal.

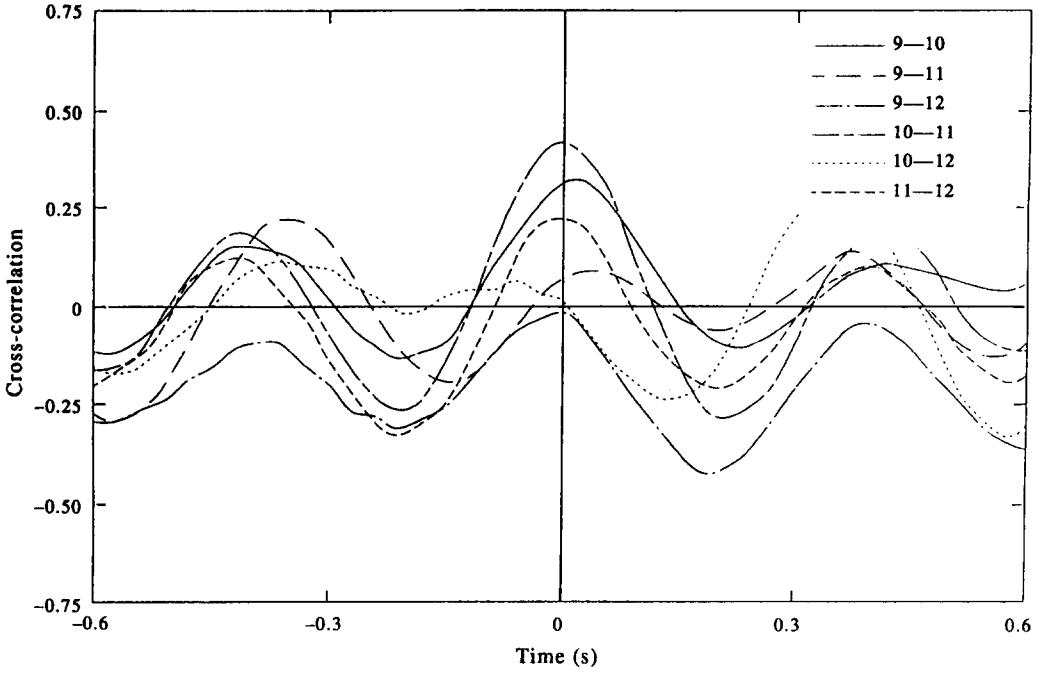


Figure 4. Cross-correlations of detector signals, 500 $\mu$m glass particles at $u_0/u_{mf} = 2$ ($u_{mf} = 21.9$ cm/s).

where $f_k = k/(N\delta t_s)$, $i = \sqrt{-1}$, and the PSD function for an average of $n_d$ sets of signals of $x_n$ is

$$S_{xx}(f_x) = \frac{1}{n_d N \delta t_s} \sum_{j=1}^{n_d} |X_j(f_k)|^2. \quad [7]$$

Figures 4 and 5 show, respectively, the cross-correlations and autocorrelations of the detector signals for the 500 $\mu$m glass particles at $u_0/u_{mf} = 2$. In figure 4, the curves for the opposite detector pairs, 9–11 and 10–12, are of particular interest. They exhibit nearly zero values of

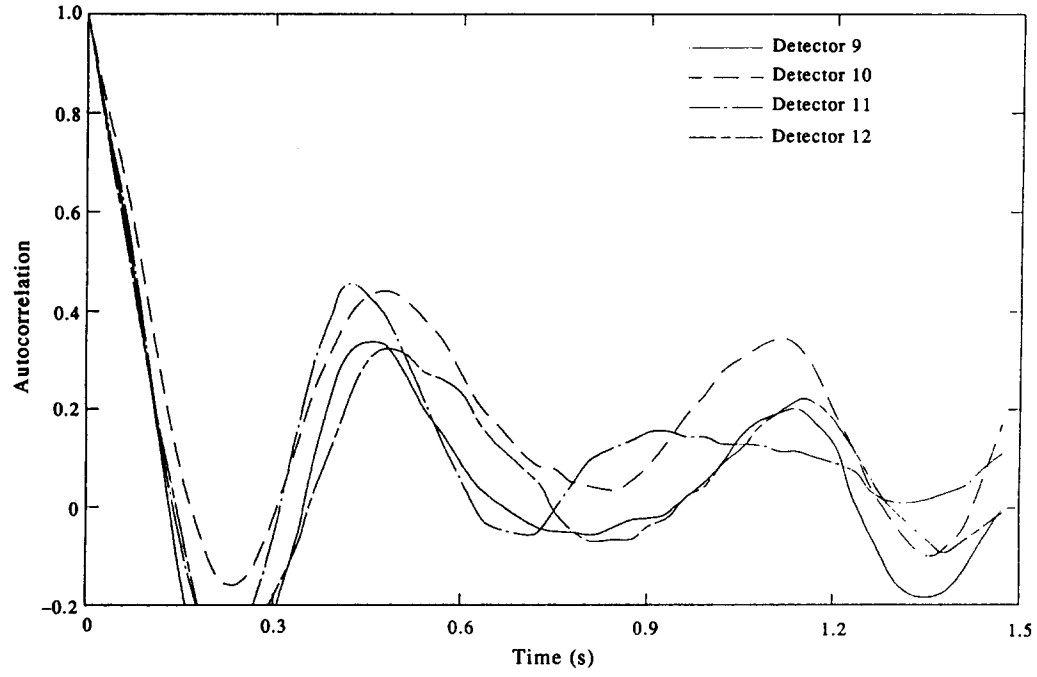


Figure 5. Autocorrelations of detector signals, 500 $\mu$m glass particles at $u_0/u_{mf} = 2$ ($u_{mf} = 21.9$ cm/s).

correlation at zero time lag, indicating significant antisymmetric sloshing motions. The curve for the adjacent detector pair, 9–12, also exhibits a nearly zero correlation at zero time lag, while that for 10–11 shows appreciable correlation. Thus, the detailed structure of the motion is quite complex. The autocorrelations, shown in figure 5, reveal the existence of both near-periodic and random fluctuations. The large-amplitude periodic oscillations of the autocorrelations represent the dominant fluctuations of the solids motion in the bed.

Figures 6(a) and (b) show the power spectra of the detector signals, respectively, for the 500 and 705 $\mu$m glass particles at $u_0/u_{mf} = 2$. Each graph represents an average of $n_d = 48$ sets of detector signals for the operating condition indicated. A significant finding is that both spectra revealed a sharp peak at about 2.5 Hz. In this study, the sampling window contained $N = 512$ data points with $\delta t_s = 30$ ms. Hence the Nyquist criterion, $1/\delta t_s \geqslant 2f_{max}$, was satisfied and aliasing should be avoided. The frequency resolution, $\delta f = 1/(N\delta t_s)$, was 0.0651 Hz.

The dominant frequencies for the 500 and 705 $\mu$m glass particles at $u_0/u_{mf} = 1.5$, 3 and 4 have also been determined and they are listed in table 2. The data for $u_0/u_{mf} = 1.5$ were evaluated from the autocorrelations since no clear sharp peak could be identified from the power spectra. Furthermore, it was also found that there was no dominant frequency when $u_0/u_{mf} > 4$. The most striking feature of the data is that the dominant frequency of the solids fluctuations, when it exists,

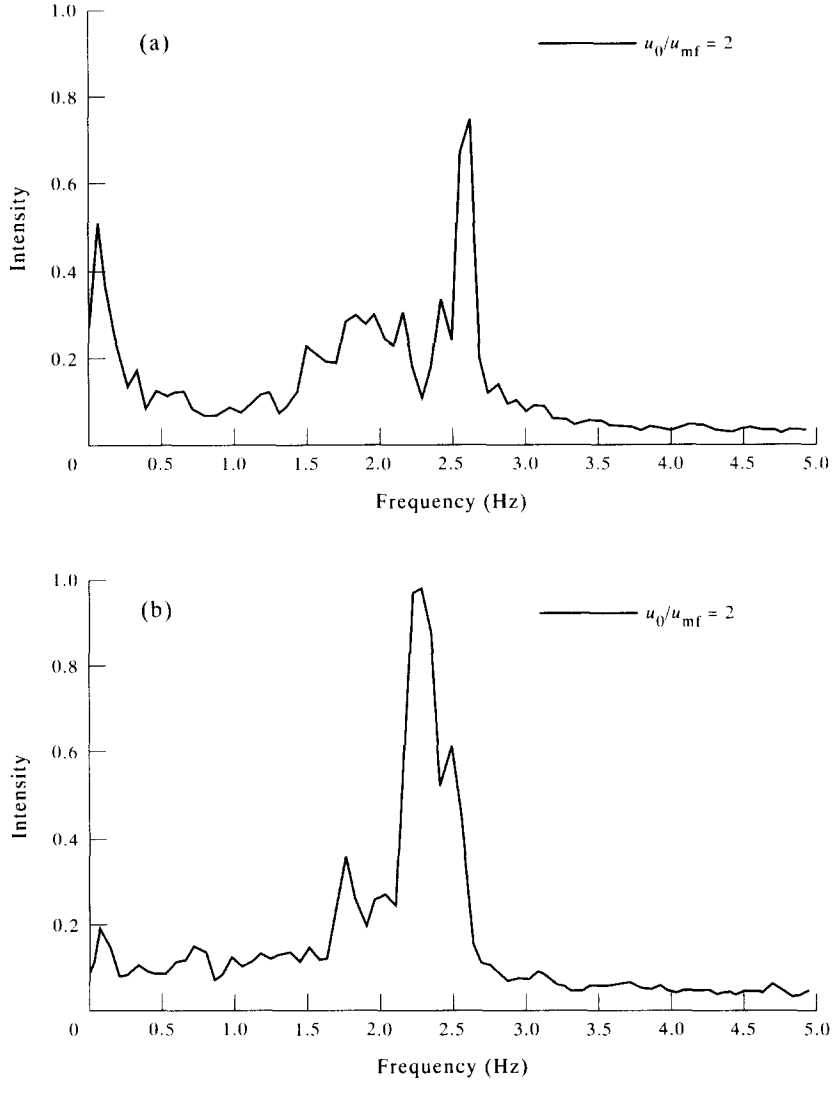


Figure 6. Averaged power spectrum of 48 sets of detector signals: (a) 500 $\mu$m glass particles at $u_0/u_{mf} = 2$ ($u_{mf} = 21.9$ cm/s); (b) 705 $\mu$m glass particles at $u_0/u_{mf} = 2$ ($u_{mf} = 30.2$ cm/s).

Table 2. Dominant fluctuation frequencies of 500 and 705 $\mu$m glass particles in a cylindrical fluidized bed of 190 mm i.d. with a static bed height of 190 mm

| | $u_0/u_{mf}$ | | | |
|---|---|---|---|---|
| $d_p(\mu m)$ | 1.5 | 2 | 3 | 4 |
| 500 | 2.15 | 2.61 | 2.48 | 2.38 |
| 705 | 2.20 | 2.28 | 2.28 | 2.48 |

is essentially independent of the particle size and the fluidization velocity, at least within the range of the variables tested.

## 4. MODELING OF SOLIDS FLUCTUATION IN FLUIDIZED BEDS

The nature of the solids global fluctuations in a fluidized bed is not clearly understood at present. In the literature, a great deal of attention was paid to the motion of bubbles. Instead, this study focuses attention on the solids sloshing motion. In what follows, evidence will be presented to show that sloshing governs the dominant fluctuations in bubbling beds of shallow and intermediate depths. Sloshing may be viewed as large-amplitude surface waves, excited by either random or coherent bed density fluctuations (bubbles) or their combination. For a cylindrical bed, the surface wave model postulates that the two modes of the solids sloshing motion, namely, the axisymmetric mode and the antisymmetric mode, are simply the full-wave and half-wave of the standing waves of the solids in a cylindrical column. The two modes of the standing waves are illustrated in figure 7. At the present time, the postulate can only be justified by the end results which show reasonable agreement with experiments. In this study, only the frequencies of the sloshing motion were analyzed.

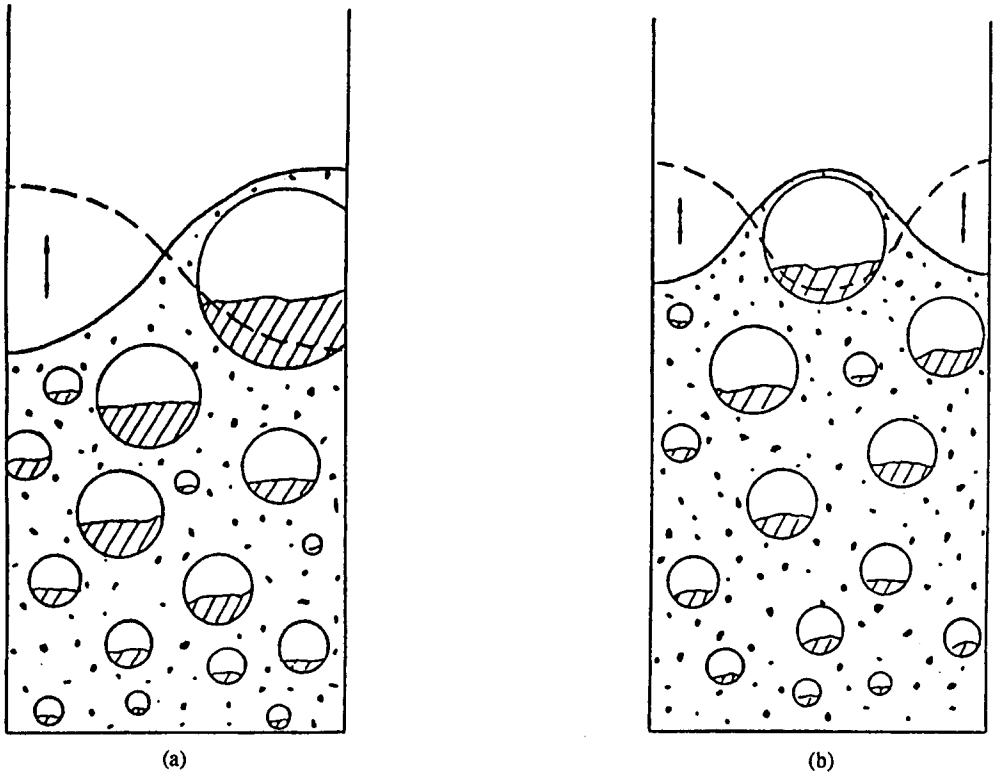


Figure 7. Standing surface waves in a cylindrical column: (a) half-wave mode; (b) full-wave mode.

### 4.1. The Standing Surface Wave Model

As a first approximation, the modes of the surface waves assimulating bed sloshings are examined by considering the bed to consist of an inviscid liquid of constant density. This simplification was motivated by the observation that the bed surface bears a strong resemblance to that filled with a single-phase liquid. The inviscid fluid assumption can be heuristically justified by the fact that bed dynamics is governed mainly by inertia-gravity balance. The constant density assumption may seem indefensible, since voidage variations and fluctuations are prominent features of a bubbling bed. However, as is shown in section 4.2, the frequency of the surface waves for a fluid with mean density variation along the height differs very little from that of fluid with constant density. It is also interesting to note that the final results based on inviscid, constant density assumption are found to be independent of density.

The linear theory of surface waves (see LeMehaute 1976) makes use of a velocity potential function $\phi$ defined by

$$\mathbf{v} = -\nabla\phi, \qquad [8]$$

where $\mathbf{v}$ is the velocity vector of the fluid. Hence, the continuity equation is

$$\nabla^2\phi = 0. \qquad [9]$$

An appropriate solution of this equation is

$$\phi = -\mathrm{B}\frac{2\pi f}{m}\frac{\cosh m(H+z)}{\sinh mH}U(\mathbf{r})\cos 2\pi ft, \quad -H \leqslant z \leqslant 0, \qquad [10]$$

where B is a positive constant related to the amplitude of the velocity fluctuation, $H$ is the fluid depth, $m$ is an eigenvalue associated with the bed geometry and wave mode, $z$ is the vertical distance from the equilibrium liquid-free surface, $f$ is the wave frequency to be determined from

$$f = \frac{1}{2\pi}(mg\tanh mH)^{1/2}, \qquad [11]$$

in which $g$ is the gravitational acceleration, and $U(\mathbf{r})$ is a function of position in the horizontal plane. It satisfies the following equation:

$$(\nabla_z^2 + m^2)U(\mathbf{r}) = 0, \qquad [12]$$

where $\nabla_z^2$ is the two-dimensional Laplacian operator in the $z$-plane. The slip boundary condition applies at the wall in accordance with the inviscid fluid assumption. For a rectangular column of widths $a$ and $b$, the solution is

$$U(\mathbf{r}) = U_{qs}(x, y) = \cos\frac{q\pi x}{a}\cos\frac{s\pi y}{b}, \quad 0 \leqslant x \leqslant a,\ 0 \leqslant y \leqslant b, \qquad [13]$$

where $q$ and $s$ are integers representing the half-wavenumbers in the $x$- and $y$-direction, respectively. The eigenvalue $m$ is given by

$$m = m_{qs} = \left[\left(\frac{q\pi}{a}\right)^2 + \left(\frac{s\pi}{b}\right)\right]^{1/2}, \quad q, s = 1, 2, \ldots. \qquad [14]$$

For a two-dimensional column, one of the integers is set to zero.

Equations [11] and [14], taken together, can be used to estimate the fluctuation frequency of rectangular and two-dimensional beds of shallow and intermediate depth when the integers $q$ and $s$ are chosen appropriately. Although the inviscid equation used here accepts all wavenumbers, in reality the dominant modes are determined by the competition between excitation and damping, and self-excitation may be a result of instabilities. In a bubbling fluidized bed, the bubbles which are themselves the consequence of instabilities are the random excitation source for the surface waves. In deep beds, the bubbles initiated at the distributor plate will have the opportunity to grow in size as they detach and move upward and eventually coalesce. As a result, more and more lower wavenumber modes get excited while the higher wavenumber modes tend to be damped to

Table 3. Values of the constants $c_{np}$

| | $n$ | | |
|---|---|---|---|
| $p$ | 0 | 1 | 2 |
| 1 | 7.663 | 3.682 | 6.108 |
| 2 | 14.03 | 10.66 | 13.41 |

a greater extent by turbulence and particulate interactions. Hence, in a deep bed we expect that the lower wavenumber modes will be dominant and $q$ and $s$ should take the value of small integers. Furthermore, the wavelengths in the two orthogonal directions in the surface plane should not be widely different in view of the nearly spherical shape of the bubbles. For a rectangular bed, this means that $a/q$ and $b/s$ in [14] should be of the same order.

For a cylindrical column of inside diameter $D$, the solution of the governing equation for $U$ in coordinates $(r, \theta)$ is

$$U(\mathbf{r}) = U_{np}(r, \theta) = J_n(m_{np}r)\cos n\theta, \quad 0 \leqslant r \leqslant D/2, \tag{15}$$

in which $n$ and $p$ are the wavenumbers. The eigenvalue $m_{np}$ is given by

$$m_{np} = \frac{c_{np}}{D}, \quad n = 0, 1, \ldots, p = 1, 2, \ldots, \tag{16}$$

where the constants $c_{np}$ are listed in table 3 for $n = 0, 1, 2$ and $p = 1, 2$.

Equations [11] and [16] may be used to estimate the frequencies of solids fluctuations in cylindrical bubbling columns. For the reasons already given, the dominant modes are those corresponding to the lowest wavenumbers. They are the full-wave or axisymmetric mode $(n = 0, p = 1)$ and the half-wave or antisymmetric mode $(n = 1, p = 1)$. It can also be shown from [15] that when $n > 1$, or $n \leqslant 1$ and $p > 1$, the function $U_{np}$ will result in triangular, kidney-shaped and other wave forms, all of which are unlikely to be excited and therefore, should be excluded. These considerations led us to conclude that for the cylindrical bed there exist only the two lowest wavenumber modes just cited.

For a cylindrical bed with $H/D$ larger than about 0.7, the frequency given by [11] and [16] becomes nearly independent of the bed height, and the lowest two wave modes are given by

$$f_\alpha = \frac{c_\alpha}{2\pi}\left(\frac{g}{D}\right)^{1/2}, \quad \alpha = 1/2, 1. \tag{17a}$$

In the above, $\alpha = 1/2$ represents the half-wave mode $(n = 1, p = 1)$ and $\alpha = 1$ represents the full-wave mode $(n = 0, p = 1)$. The two constants $c_{1/2}$ and $c_1$ can be evaluated from table 3, and they are $(3.682)^{1/2} = 1.92$ and $(7.663)^{1/2} = 2.77$, respectively. Baeyens & Geldart (1974) indicated that slugging would occur when $H/D > 2$ (for $D < 0.4$ m). Hence, [17a] is expected to be applicable to fluidized beds of intermediate depth, namely, $0.7 < H/D < 2$, since the present analysis pertains to bubbling beds only.

The velocity fields of the first two modes of fluctuations may be derived from [8], [10] and [13] or [15], depending on whether the bed has a rectangular or cylindrical cross section. In the interest of conserving space, only the results for the cylindrical bed are given. For the half-wave mode, $\alpha = 1/2$, the velocity components are:

$$v_r = 2\pi B_1 f_{11} \frac{\cosh m_{11}(H + z)}{\sinh m_{11} H}\left[J_0(m_{11}r) - \frac{1}{m_{11}r}J_1(m_{11}r)\right]\cos\theta \cos 2\pi f_{11} t, \tag{18a}$$

$$v_\theta = -2\pi B_1 f_{11} \frac{\cosh m_{11}(H + z)}{\sinh m_{11} H}\frac{1}{m_{11}r}J_1(m_{11}r)\sin\theta \cos 2\pi f_{11} t \tag{18b}$$

and

$$v_z = 2\pi B_1 f_{11} \frac{\sinh m_{11}(H + z)}{\sinh m_{11} H}J_1(m_{11}r)\cos\theta \cos 2\pi f_{11} t, \tag{18c}$$

where $m_{11}D = c_{11}$. For the full-wave mode, $\alpha = 1$, they are:

$$v_r = -2\pi B_0 f_{01} \frac{\cosh m_{01}(H+z)}{\sinh m_{01}H} J_1(m_{01}r)\cos 2\pi f_{01}t, \quad [19a]$$

$$v_\theta = 0 \quad [19b]$$

and

$$v_z = 2\pi B_0 f_{01} \frac{\sinh m_{01}(H+z)}{\sinh m_{01}H} J_0(m_{01}r)\cos 2\pi f_{01}t, \quad [19c]$$

where $m_{01}D = c_{01}$. It is seen that the velocity field of the half-wave mode, [18], is antisymmetric and that of the full-wave mode, [19], is axisymmetric.

In a shallow fluidized bed, the bubbles will not have the opportunity to coalesce to form a single bubble as depicted in figure 7. Many smaller bubbles will erupt at the bed surface. Under such circumstances, the bed diameter is no longer a relevant length scale. Each bubble cell in the bed surface can be viewed as a full-wave mode and its frequency may be used to estimate the fluctuation frequency in shallow beds. Accordingly, we set $\alpha = 1$ and replace $D$ in [17a] by a wavelength $\lambda$. Hence,

$$f = \frac{c_1}{2\pi}\left(\frac{g}{\lambda}\right)^{1/2}. \quad [17b]$$

The wavelength $\lambda$ may be determined from experiments or analysis. When $\lambda$ is not available, it can be estimated from the bubble diameter at the bed surface. From a consideration of the mass balance for the particles in the surface region, $\lambda$ should be at least twice the bubble diameter. Thus, the proposed standing surface wave model led us to conclude that, in general, the fluctuation frequency of bubbling fluidized beds of intermediate depths and of shallow beds is given by

$$f_\alpha = \frac{c_\alpha}{2\pi}\left(\frac{g}{L}\right)^{1/2}, \quad [20]$$

where $\alpha$ refers to wave mode, $g$ is the gravitational acceleration and $L$ is a length scale. The numerical constant $c_\alpha$ can be determined theoretically as has been illustrated. For cylindrical beds of intermediate depth ($2.0 > H/D > 0.7$), $L$ is the bed diameter $D$, and for shallow beds, $L$ is the wavelength $\lambda$. There is no empiricism involved. We note that this result cannot be obtained from dimensional analysis.

An examination of [11], [14], [16] and [20] shows that the predicted frequencies depend only on the bed height, bed size (diameter for cylindrical beds, length of two sides for rectangular beds, and width for two-dimensional beds), and, for shallow beds, a characteristic wavelength $\lambda$. The fluid density does not appear in any of these equations. Within limits, the particle properties (density, size and shape) and the superficial gas velocity do not have a direct effect. They play a role in shallow beds via their influence on the wavelength. It is therefore seen that, for bubbling fluidized beds of shallow and intermediate depths, although the excitation force for bed fluctuations originates from bubbles, the fluctuation frequency and the bubble frequency at "resonance" are controlled by the surface waves. The physics of the waves is not dominated by the bubbles. It is the surface wave, not bubbles, that is responsible for the frequency of solids fluctuations in bubbling fluidized beds.

Another result of this study is that, for a bed with a fixed depth, there exists a minimum frequency, $f_{1/2}$ given by [20], of the solids sloshing motion. For a bed of sufficient depth, this frequency is also that of the big bubbles rising and bursting at the bed surface.

### *4.2. Surface Waves in Inviscid Fluid of Nonuniform Density*

Among the several assumptions used in the analysis of section 4.1, that of constant density would appear to be the most objectionable. In this section, we examine the influence of nonuniform density on the predicted frequency of the surface waves.

*4.2.1. Basic assumptions and governing equations*

We consider small-amplitude surface waves in an otherwise stationary fluid whose mean density $R$ is a function of the vertical position $z$ only,

$$R \equiv \langle \rho^*(x, y, z, t) \rangle = R(z), \tag{21}$$

where $\langle\ \rangle$ denotes the space-time average over a horizontal plane. The free surface height will be denoted by $\zeta^*(x, y, t)$. The $z$-coordinate is positive downward, with the origin chosen so that the average surface height is zero, i.e.

$$\langle \zeta^*(x, y, t) \rangle = 0. \tag{22}$$

For convenience, the flow variables, $\rho^*$, the velocity vector $\mathbf{u}^*$ (or equivalently, its components $u^*$, $v^*$, $w^*$), the static pressure $p^*$ and $\zeta^*$ are denoted with asterisks. The continuity equation for the fluid is

$$\frac{\mathrm{D}\rho^*}{\mathrm{D}t} + \rho^* \nabla \cdot \mathbf{u}^* = 0. \tag{23}$$

We consider the simple case that the fluid is incompressible. However, if an equation of state can be prescribed for a particular fluid, this simplification can be lifted. The incompressibility assumption implies that

$$\frac{\mathrm{D}\rho^*}{\mathrm{D}t} = 0, \tag{24a}$$

and hence, the continuity equation becomes

$$\nabla \cdot \mathbf{u}^* = 0. \tag{24b}$$

Note that the assumption of incompressibility does not preclude the density variation as described by [21]. The momentum equation for the fluid is

$$\rho^* \frac{\mathrm{D}\mathbf{u}^*}{\mathrm{D}t} = -\nabla p^* + \mathbf{k}\rho^* g, \tag{25}$$

where $\mathbf{k}$ is the unit vector in the $z$-direction and $g$ is the gravitational acceleration. The dynamic boundary condition for the fluid at $z = \zeta^*$ is

$$p^*(x, y, \zeta^*, t) = 0 \tag{26}$$

and the kinematic boundary condition is

$$w^*(x, y, \zeta^*, t) = \frac{\partial \zeta^*(x, y, t)}{\partial t}. \tag{27}$$

Since the fluid is inviscid, boundary conditions are not needed for the velocities $u^*$ and $v^*$.

The flow variables, $\rho^*$, $\mathbf{u}^*$, $p^*$ and $\zeta^*$, are decomposed into their respective mean and oscillating components, to be denoted by upper- and lower-case characters (English or Greek), as follows:

$$\rho^*(x, y, z, t) = R(z) + \rho(x, y, z, t), \tag{28}$$

$$p^*(x, y, z, t) = P(z) + p(x, y, z, t), \tag{29}$$

$$\mathbf{u}^*(x, y, z, t) = \mathbf{u}(x, y, z, t), \tag{30}$$

and

$$\zeta^*(x, y, t) = \zeta(x, y, t). \tag{31}$$

Substituting [28]–[31] into the governing equations [24b] and [25] and making use of the boundary conditions [26] and [27], one finds that for the mean flow only the pressure $P$ is nontrivial. It is given by

$$P(z) = g \int_0^z R(z)\, \mathrm{d}z. \tag{32}$$

*4.2.2. Linearized governing equations and boundary conditions for oscillating components*

The substitution just described also leads to the following linearized equations for $\rho$, $\mathbf{u}$, $p$ and $\zeta$. The incompressibility condition becomes

$$\frac{D\rho}{Dt} + wR' = 0, \tag{33}$$

where $R' \equiv dR/dz$. The continuity equation is unchanged:

$$\nabla \cdot \mathbf{u} = 0. \tag{34}$$

The $x$- and $y$-momentum equations are

$$R\frac{\partial u}{\partial t} = -\frac{\partial p}{\partial x} \tag{35}$$

and

$$R\frac{\partial v}{\partial t} = -\frac{\partial p}{\partial y}, \tag{36}$$

and the $z$-momentum equation becomes

$$R\frac{\partial w}{\partial t} = -\frac{\partial p}{\partial z} + \rho g. \tag{37}$$

The boundary conditions [26] and [27] are transposed to $z = 0$ by performing a Taylor series expansion with the small parameter $\zeta$. The results are

$$p(x, y, 0, t) = -gR(0)\zeta \tag{38}$$

and

$$w(x, y, 0, t) = \frac{\partial \zeta}{\partial t}. \tag{39}$$

*4.2.3. Wave frequency based on linearized equations*

For brevity, we consider two-dimensional flows ($v = 0$). The procedure can be formally extended to three-dimensional flows. The normal mode of the progressive surface wave is assumed to be of the form:

$$w = e^{ikx - ivt}h(z), \tag{40}$$

where $i = \sqrt{-1}$, $k$ is the wavenumber and $v$ is the frequency. One readily obtains from [34],

$$u = \frac{i}{k} e^{ikx - ivt}h', \tag{41}$$

where $h' = dh/dz$; from [33],

$$\rho = -\frac{i}{v} e^{ikx - ivt}R'h; \tag{42}$$

and from [35],

$$p = i\frac{v}{k^2} e^{ikx - ivt}Rh'. \tag{43}$$

Substituting [41]–[43] into [37] and rearranging leads to

$$h'' + \frac{R'}{R}h' - \left(1 - \frac{g}{v^2}\frac{R'}{R}\right)k^2 h = 0, \tag{44}$$

where $h'' = d^2h/dz^2$. From the kinematic boundary condition [39], we obtain

$$\zeta = \frac{i}{v} e^{ikx - ivt}h(0). \tag{45}$$

Introducing [45] into [38] and equating the result to [43], for $z = 0$, gives

$$\frac{h'(0)}{h(0)} = -\frac{k^2}{v^2}g. \qquad [46]$$

Introducing a dimensionless parameter $L \equiv g/v^2H$, where $H$ is the mean bed height, and a dimensionless coordinate $\xi = z/H$, [44] becomes

$$h'' + \frac{R'}{R}h' - \left(1 - L\frac{R'}{R}\right)k^2H^2h = 0, \qquad [47]$$

in which the prime now denotes differentiation with respect to $\xi$.

Ai (1991) measured the time-averaged solids volume fraction in a rectangular, atmospheric fluidized bed, $38 \times 400$ mm in cross section, with 425–500 $\mu$m glass spheres. The minimum fluidization velocity determined from pressure drop measurements was 20.1 cm/s. It was found that the mean solids density $R$ increases as $\xi$ increases from 0 to $\xi_j(<1)$, beyond which $R$ becomes essentially a constant. In the region $0 \leqslant \xi \leqslant \xi_j$, the data can be well-fitted by a second degree polynomial:

$$R(\xi) = R(0)(1 + m_1\xi + m_2\xi^2), \quad 0 \leqslant \xi \leqslant \xi_j, \qquad [48]$$

where the numerical coefficients $m_1$, $m_2$ and $\xi_j$ depend on the fluidizing velocity. It is to be noted that the solution of [47] depends only on the ratio $R'/R$ and hence the value $R(0)$ is of no consequence.

*Solution for region I ($0 \leqslant \xi \leqslant \xi_j$).* Introducing [48] into [47], the latter becomes

$$(1 + m_1\xi + m_2\xi^2)h_1'' + (m_1 + 2m_2\xi)h_1' - [(1 + m_1\xi + m_2\xi^2) - L(m_1 + 2m_2\xi)]k^2H^2h_1 = 0. \qquad [49]$$

We consider a series solution of the form

$$h_1 = a_0 + a_1\xi + a_2\xi^2 + a_3\xi^3 + a_4\xi^4 + \cdots. \qquad [50]$$

Substituting [50] into [49], combining terms in like powers of $\xi$ and setting their coefficients to zero yield the following relations:

$$2a_2 + m_1a_1 - k^2H^2(1 - Lm_1)a_0 = 0, \qquad [51a]$$

$$6a_3 + 4m_1a_2 + [2m_2 - k^2H^2(1 - Lm_1)]a_1 - k^2H^2(m_1 - 2Lm_2)a_0 = 0, \qquad [51b]$$

and

$$(n + 2)(n + 1)a_{n+2} + (n + 1)^2m_1a_{n+1} + [(n + 1)nm_2 - k^2H^2(1 - Lm_1)]a_n - k^2H^2(m_1 - 2Lm_2)a_{n-1} - k^2H^2m_2a_{n-2} = 0, \quad \text{for } n \geqslant 2. \qquad [51c]$$

Equation [46] requires that

$$\frac{a_1}{a_0} = -Lk^2H^2 \qquad [52a]$$

and hence, from [51],

$$\frac{a_2}{a_0} = \tfrac{1}{2}k^2H^2, \qquad [52b]$$

$$\frac{a_3}{a_0} = -\tfrac{1}{6}k^2H^2[m_1 + Lk^2H^2(1 - Lm_1)], \qquad [52c]$$

$$\frac{a_4}{a_0} = \tfrac{1}{12}k^2H^2\left[\left(\tfrac{3}{2}m_1^2 - 2m_2\right)(1 - L^2k^2H^2) + \tfrac{1}{2}k^2H^2\right] \qquad [52d]$$

etc. Thus, the solution for region I is

$$h_1 = a_0\{1 - Lk^2H^2\xi + \tfrac{1}{2}k^2H^2\xi^2 - \tfrac{1}{6}k^2H^2[m_1 + Lk^2H^2(1 - Lm_1)]\xi^3 + \tfrac{1}{12}k^2H^2\left[\left(\tfrac{3}{2}m_1^2 - 2m_2\right)(1 - L^2k^2H^2) + \tfrac{1}{2}k^2H^2\right]\xi^4 - \cdots\}. \qquad [53]$$

*Solution for the region II ($\xi_j \leqslant \xi \leqslant 1$).* In this region, $R$ is essentially uniform and $R' = 0$. The governing equation is

$$h_{II}'' - k^2H^2h_{II} = 0. \quad [54]$$

The solution which satisfies the boundary condition $h_{II}(1) = 0$ is

$$h_{II} = b_0 \sinh kH(1 - \xi). \quad [55]$$

To join the two solutions in regions I and II, we impose the condition that the velocities $u$ and $w$, the density $\rho$ and the pressure $p$ are continuous at $\xi = \xi_j$. This requires that $h_I(\xi_j) = h_{II}(\xi_j)$ and $h_I'(\xi_j) = h_{II}'(\xi_j)$ which, taken together, lead to:

$$\frac{1 - Lk^2H^2\xi_j + \frac{1}{2}k^2H^2\xi_j^2 - \frac{1}{6}k^2H^2[m_1 + Lk^2H^2(1 - Lm_1)]\xi_j^3 + \frac{1}{12}k^2H^2[(\frac{3}{2}m_1^2 - 2m_2)(1 - L^2k^2H^2) + \frac{1}{2}k^2H^2]\xi_j^4 - \cdots}{L - \xi_j + \frac{1}{2}[m_1 + Lk^2H^2(1 - Lm_1)]\xi_j^2 - \frac{1}{3}[(\frac{3}{2}m_1^2 - 2m_2)(1 - L^2k^2H^2) + \frac{1}{2}k^2H^2]\xi_j^3 + \cdots} = kH \tanh kH(1 - \xi_j). \quad [56]$$

Equation [56] is the desired relation between $L(\equiv g/v^2H)$ and $kH$, if the two series in the numerator and denominator converge. To be consistent with the linear analysis (small-amplitude waves), the use of [56] should probably be limited to small $\xi_j$ and the series would be convergent. When the series are semidivergent, Euler's method can be used to determine the sum.

When the mean density is uniform throughout the bed, $\xi_j = 0$, [56] simplifies to

$$v^2 = kg \tanh kH, \quad [57]$$

which is the same as [11] with $m = k$ and $v = 2\pi f$.

*4.2.4. Comparison of wave frequency in a variable and uniform density two-dimensional column*

To examine the influence of the solids density variation on the wave frequency of a bubbling bed, we consider a two-dimensional column having a height $H = 0.625$ m and a width $W = 0.625$ m. The lowest wave mode has a wavelength $1/k = W/\pi$. From [57], the corresponding circular frequency is $v_0 = 6.99\ s^{-1}$.

At $u_0/u_{mf} = 1.94$, Ai's (1991) measured mean density data showed that:

$$\frac{R(\xi)}{R(0)} = 1 + 13\xi - 8.47\xi^2, \quad 0 < \xi < \xi_j \quad [58a]$$

and

$$\frac{R(\xi)}{R(0)} = 6.0, \quad \xi_j < \xi < 1, \quad [58b]$$

with $\xi_j = 0.768$, as shown in figure 8. Using 30 terms in [56], and employing Euler's method of computing the sum, we obtain $v = 6.97\ s^{-1}$. When 50 terms were used, the calculated $v$ remained the same up to the second decimal place.

Next we consider a smaller variation of the bed density which would occur at a lower fluidizing velocity. Specifically, we set

$$\frac{R(\xi)}{R(0)} = 1 + 3\xi - 7.5\xi^2, \quad 0 < \xi < \xi_j \quad [59a]$$

and

$$\frac{R(\xi)}{R(0)} = 1.3, \quad \xi_j < \xi < 1, \quad [59b]$$

with $\xi_j = 0.2$. This variation is also illustrated in figure 8. Using 30 terms in [56], we obtain $v = 6.99\ s^{-1}$, the same as $v_0$. The foregoing two examples clearly demonstrate that the variation of the mean fluid density has very little effect on the frequency of the surface waves.

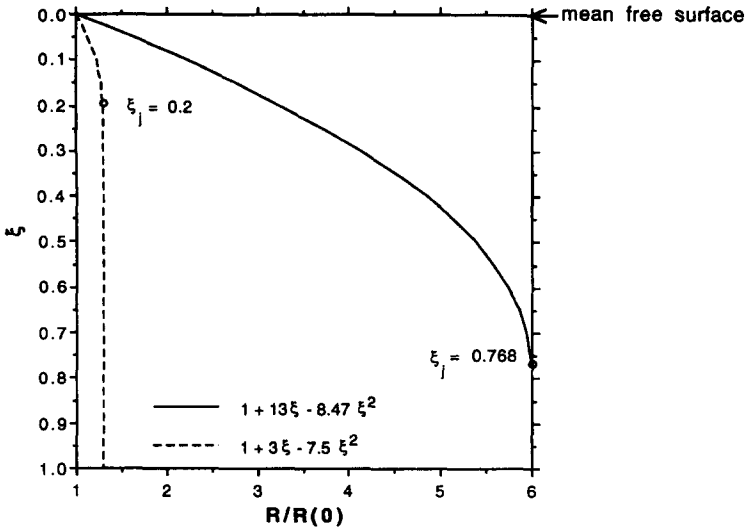


Figure 8. Variation of the average solids density with depth.

### 4.3. *Comparison with the Experimental Data*

#### 4.3.1. *Cylindrical fluidized beds of intermediate depth*

The experimental results of the bed fluctuation frequencies, listed in table 2, can be compared with the model predictions. Since $D = 190$ mm and the expanded bed height is approximately 200 mm, [17a] is applicable. The predicted frequencies for the two modes are: $f_{1/2} = (1.92/2\pi)(9810/190)^{1/2} = 2.19$ Hz and $f_1 = (2.77/2\pi)(9810/190)^{1/2} = 3.16$ Hz. The measured dominant frequencies listed in table 2 are well within the predictions.

In figure 9, reported experimental results of a large number of investigators (Hiby 1967; Kunii *et al.* 1967; Lirag & Littman 1971; Wong & Baird 1971; Baird & Klein 1973; Baeyens & Geldart 1974; Verloop & Heertjes 1974; Broadhurst & Becker 1976; Fan *et al.* 1981; Svoboda *et al.* 1983, 1984; Noordergraaf *et al.* 1987; Rockey *et al.* 1989) together with the measured results

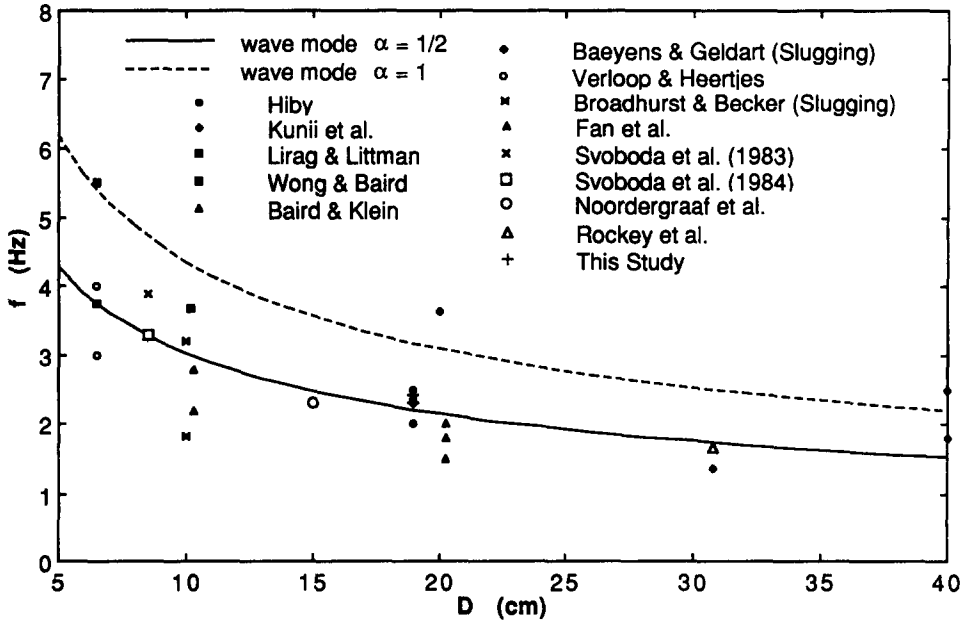


Figure 9. Comparison of the predicted frequency with the experimental data for cylindrical beds of intermediate depth, $0.7 < H/D < 2$.

of this study are compared with the model predictions. The operating conditions for the experiments are summarized in table 4. The particle sizes and particle densities used in these studies ranged, respectively, from 58 to 3180 $\mu$m and from 1.1 to 8.56 g/cm$^3$. Since [17a] is valid for bed depths in the approximate range $0.7 < H/D < 2$, the data plotted in figure 9 are in this range. It is seen that the model agrees fairly well with the data, considering the very wide range of bed sizes, particle properties and operating conditions. The data of Baeyens & Geldart (1974) and of Broadhurst & Beckder (1976) were for slugging beds. Had these been deleted in figure 9, the comparison would look even better. They are included for the purpose of illustrating that the slugging frequency is generally lower than the sloshing frequency for beds of same geometry. This observation is generally in agreement with the results of Svoboda *et al.* (1983, 1984), Noordergraaf *et al.* (1987) and Rockey *et al.* (1989). We shall return to this point later.

### *4.3.2. Shallow cylindrical fluidized beds*

The predictions of [17b] can be compared with the experimental data reported in the literature for shallow beds. Since information on the characteristic wavelength $\lambda$ was not available, it was evaluated from the estimated bubble diameters. However, this does not mean that the bed frequency is determined by the bubble diameter. In fact, there is no unique correlation between $\lambda$ and bubble diameter as will be shown later. In figure 10a the experimental data of Lirag & Littman (1971) and Fan *et al.* (1981) are compared with the predicted frequencies with bubble diameters calculated from the empirical correlation of Kato & Wen (1969). In these experiments, the particle diameter ranged from 130 to 700 $\mu$m, the particle density ranged from 2.4 to 7.7 g/cm$^3$ and the aspect ratio $H/D$ ranged from 0.12 to 0.7 for the Lirag & Littman bed and from 0.3 to 0.49 for the Fan *et al.* bed. Since the Kato & Wen's correlation is valid when the bubble growth is not affected by the bed wall, its use is limited to bubble diameters smaller than about one-quarter of the bed diameter (Baeyens & Geldart 1974). Therefore, in figure 10a, only those data for which the calculated bubble diameter was less than half the bed diameter were used. The theoretical

Table 4. Solids fluctuation frequencies in cylindrical beds of intermediate depth

| Reference | $D$ (cm) | $H$ (cm) | Particle | $\rho_p$ (g/cm$^3$) | $d_p$ ($\mu$m) | $u_{mf}$ (cm/s) | $u_0/u_{mf}$ | $f$ (Hz) |
|---|---|---|---|---|---|---|---|---|
| Hiby (1967) | 19 | 16.5 | Glass | 2.41 | 900–1200 | | 1.5 | 2.35 |
| | | 13.2 | Sand | 1.66 | 1000–1200 | | 1.5 | 2.5 |
| | | 20.3 | | | | | 1.5 | 2.3 |
| | | 29.7 | | | | | 1.5–2.3 | 2.0 |
| Kunii *et al.* (1967) | 20 | 30 | Catalyst | 1.54 | 150 | 2 | 3.4–8.5 | 3.65 |
| | 40 | 50 | | | | | 5.6 | 1.8 |
| | | | | | | | >8 | 2.5 |
| Lirag & Littman (1971) | 6.5 | 10.5 | Glass | 2.42 | 500 | 19.1 | 1.23 | 3.75 |
| | | 8.4 | | 2.48 | 318 | 7.09 | 1.23 | 5.5 |
| Wong & Baird (1971) | 10.2 | 11.2 | Glass | 2.5 | 390–470 | 12.2 | 1.5 | 3.7 |
| Baird & Klein (1973) | 10.3 | 8.2–20.4 | Glass | 2.49 | 254 | 3.6 | >2 | 2.2 |
| | | 8.5 | Hematite | 5.72 | 563 | 21.5 | >2.2 | 2.8 |
| Baeyens & Geldart (1974) | 30.8 | 35 | Catalyst sand | 1.17–2.65 | 58–1848 | | High | 1.36 |
| Verloop & Heertjes (1974) | 6.5 | 5.3 | Copper | 8.56 | 370 | 29.5 | 1.2–1.4 | 4.0 |
| | | 8.8 | | | 460 | 39.5 | 1.2–2 | 3.0 |
| Broadhurst & Becker (1976) | 10 | 10 | Sand | 2.66 | 71–213 | | | 3.21 |
| | | 20 | | | | | | 1.81 |
| Fan *et al.* (1981) | 20.3 | 35 | Sand | 2.64 | 711 | 36.8 | 2 | 2.0 |
| | | 40 | | | | | 1.5–2 | 1.5 |
| | | 40 | | 2.62 | 491 | 14 | 1.5–2 | 1.8 |
| Svoboda *et al.* (1983) | 8.5 | 17 | Lime | 1.34 | 900 | 30.8 | 1.5 | 3.9 |
| Svoboda *et al.* (1984) | 8.5 | 17 | Limestone | 2.22 | 565 | 24.2 | 1.07–1.55 | 3.3 |
| Noordergraaf *et al.* (1987) | 15 | 31 | Glass | 2.80 | 450–540 | 23.0 | 1.5–3 | 2.3 |
| Rockey *et al.* (1989) | 30.8 | 46 | Nylon | 1.1 | 3180 | 100 | 2.6–5 | 1.65 |
| This study | 19 | 19 | Glass | 2.50 | 500 | 21.9 | 1.5–4 | 2.41 |
| | | | | | 705 | 30.2 | 1.5–4 | 2.31 |

predictions are shown for $\lambda = 3D_B$ and $\lambda = 2D_B$. The reasons for the choice are as follows. Experimental results obtained by Botterill *et al.* (1966) showed that the extent of the surface disturbance which corresponds to half the wavelength is about 1.5 times the bubble diameter. Hence $\lambda = 3D_B$. On the other hand, the lower limit of $\lambda$ is $2D_B$ as has been stated earlier. It is seen from figure 10a that the predicted frequency based on $\lambda = 3D_B$ exhibits a reasonable agreement with the experimental data. For beds of intermediate depth, the antisymmetric and axisymmetric frequencies $f_{1/2}$ and $f_1$ depend only on the bed diameter and are independent of $D_B$. For comparison

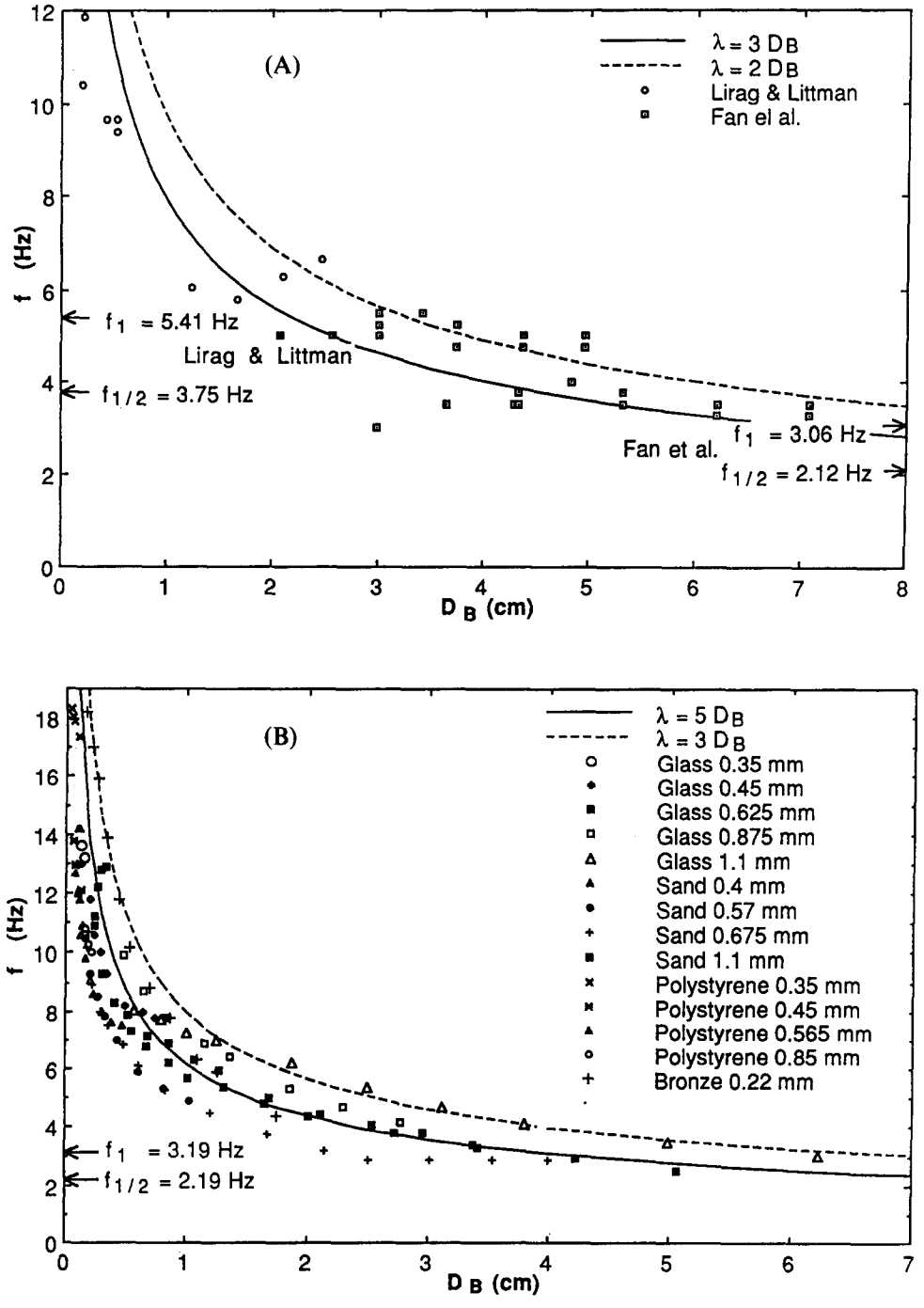


Figure 10. (A) Comparison of the predicted frequency with the experimental data for shallow cylindrical beds. (B) Comparison of the predicted frequency with Hiby's (1967) experimental data for a shallow cylindrical bed.

Table 5. Solids fluctuation frequencies in square and rectangular beds of intermediate depth

| Reference | Bed size ($cm^2$) | $H$ (cm) | Particle | $\rho_p$ ($g/cm^3$) | $d_p$ ($\mu m$) | $u_{mf}$ (cm/s) | $u_0/u_{mf}$ | $f$ (Hz) | From model† $f_{01}$ | $f_{11}$ | $f_{12}$ | $f_{22}$ |
|---|---|---|---|---|---|---|---|---|---|---|---|---|
| Botterill *et al.* (1966) | 5 × 7.5 | 7 | Bollotine | 2.5 | 200 | 2.3 | | 8 | 3.22 | 4.33 | 5.10 | 6.12 |
| | | 7 | Sand | 2.62 | 50 | 0.95 | | 7.5 | | | | |
| Goossens (1976) | 10 × 10 | 10 | | | | | 2–3 | 7 | 2.79 | 3.32 | 4.18 | 4.70 |
| | | 20 | | | | | | 3.4 | | | | |
| Canada *et al.* (1978) | 10.5 × 30.5 | 25 | Glass | 2.48 | 650 | 30 | 2.03 | 1.28 | 1.60 | 2.80 | 3.00 | 3.97 |
| | | | | | | | 2.33 | 1.33 | ($f_{02}$ = 2.26) | | ($f_{03}$ = 2.77) | |
| | | | | | | | 4.07 | 1.54 | | | | |
| | | 40 | | | | | 2.03 | 0.91 | | | | |
| | | | | | | | 3.27 | 0.95 | | | | |
| | | | | | | | 4.6 | 1.0 | | | | |
| | | | | 2.92 | 2600 | 130 | 3.31 | 1.25 | | | | |
| | 61 × 61 | 70 | | 2.48 | 650 | 30 | 3.07 | 0.71 | 1.13 | 1.34 | 1.69 | 1.90 |
| | | | | | | | 5 | 0.95 | | | | |
| | | | | 2.92 | 2600 | 130 | 1.38 | 0.67 | | | | |
| Ai (1991) | 30.5 × 30.5 | 40.6 | Glass | 2.50 | 425–600 | 21.9 | 2.37 | 2.10‡ | 1.60 | 1.90 | 2.39 | 2.69 |

†The predicted frequency $f_{qs}$ is evaluated from [11] and [14].
‡Average of 30 locations in the square bed, frequency ranged from 1.77 to 2.56 Hz.

Table 6. Solids fluctuation frequencies in two-dimensional beds of intermediate depth

| Reference | Bed size ($cm^2$) | $H$ (cm) | Particle | $\rho_p$ ($g/cm^3$) | $d_p$ ($\mu m$) | $u_{mf}$ (cm/s) | $u_0/u_{mf}$ | $f$ (Hz) | From model† $f_{01}$ | $f_{02}$ | $f_{03}$ | $f_{04}$ |
|---|---|---|---|---|---|---|---|---|---|---|---|---|
| Kunii *et al.* (1967) | 80 × 6.3 | 83 | Catalyst | 1.54 | 150 | 2 | 6.8–17 | 1.8 | 0.99 | 1.40 | 1.71 | 1.97 |
| Didwania & Homsy | 30 × 3.15 | | | 3.99 | 590 | | | 1.5–2.2 | 1.61 | 2.28 | 2.79 | 3.22 |
| (1981b)‡ | | | | 3.99 | 1100 | | | 1.6–2.3 | | | | |

†The predicted frequency $f_{qs}$ is evaluated from [11] and [14].
‡Liquid fluidized bed.

purposes they have been evaluated for the beds of Lirag & Littman (1971) and Fan *et al.* (1981). The results are shown by arrows in figure 10a. Hiby (1967) reported the fluctuation frequencies of a shallow bed for a number of particle sizes and particle densities at different heights ($0.022 < H/D < 0.52$). Figure 10b compares Hiby's data with the prediction of [17b] with $\lambda = 3D_B$ and $5D_B$. The latter was included since the calculated bubble diameters based on the Kato & Wen's correlation were found to be unrealistically small, being only a few particle diameters. Again, for comparison purposes, the two frequencies, $f_1$ and $f_{1/2}$, for Hiby's bed are shown by the arrows in figure 10b.

If one assumes that $\lambda$ is proportional to $D_B$ and hence is proportional to $H$ according to Kato & Wen's correlation for a bed with a porous distributor plate, then [17b] shows that $f$ is proportional to $(g/H)^{1/2}$. This results in a prediction for the fluctuation frequency in shallow beds, which is the same as that developed by Verloop & Heertjes (1974), [1].

#### *4.3.3. Rectangular and two-dimensional beds*

The experimental results of Botterill *et al.* (1966), Goossens (1976), Canada *et al.* (1978) and Ai (1991) for the solids fluctuation frequencies in square and rectangular beds are summarized in table 5 along with the operating conditions. The predicted frequencies, $f_{qs}$, are calculated from [11] and [14] for several sets of $(q, s)$ values. It is seen that the predictions qualitatively agree with the measurements. For two-dimensional beds, the results of Kunii *et al.* (1967) and Didwania & Homsy (1981b) for a liquid–solid bed, are shown in table 6. The predicted frequencies are also calculated from [11] and [14] with $q = 0$ and $s$ as the half-wavenumber. Here the predictions are fair.

## 5. DISCUSSION

This paper makes a distinction between the sloshing and slugging motions of a fluidized bed. Slugging can be viewed as plain gas void (slug) traveling upward with solids in plug formation oscillating vertically in a one-dimensional column. The motion is more appropriately modeled by traveling waves. This contrasts with the standing surface wave model for the sloshing motion considered in this study. Depending on the experimental conditions, one of the mechanisms may be dominant. Sloshing fluctuations usually exist in shallow beds and beds of intermediate depth. Deep beds are conducive to slugging. When this occurs, the slugging models of Verloop & Heertjes (1974) and Baeyens & Geldart (1974) can be used. These models show that the slugging frequency decreases approximately linearly with the bed height and becomes invariant beyond a critical height. For shallow fluidized beds, on the other hand, sloshing is the dominant mechanism and the bed height plays no role in the sloshing frequency. For beds of intermediate depth, both sloshing and slugging may be operative, with sloshing being the dominant mechanism at the shallow end. It transits to slugging as the depth increases. More research is needed to delineate the transition as influenced by the bed parameters. In the following, experimental results in the literature are examined further and interpreted and they lend support to the standing surface wave model.

Svoboda *et al.* (1983, 1984) measured the solids fluctuation frequencies in a cylindrical fluidized bed of 8.5 cm i.d. with $H/D = 2$. For corundum particles of 715 $\mu$m mean diameter at $u_0/v_{mf} = 1.2$, two distinct frequencies could be identified from the power spectrum, one at about 2.0 Hz and the other at about 3.9 Hz (Svoboda *et al.* 1983, figure 4). For limestome particles of mean diameter 565 $\mu$m, the two frequencies were approximately 2.1 Hz, which varied slightly with gas velocity, and 3.3 Hz, which was independent of gas velocity (Svoboda *et al.* 1984, table 2). At low gas velocities, $u_0/u_{mf} < 1.2$, the higher frequency was dominant. With increasing gas velocities, $u_0/u_{mf} > 1.36$, the lower frequency became dominant and the bed was observed in slugging fluctuations. From the standing surface wave model one finds $f_{1/2} = 3.28$, which is close to the measured frequency when the bed was not slugging. Hence, one may conclude that the observed higher frequency is associated with sloshing and the lower one with slugging.

Noordergraaf *et al.* (1987) measured the fluctuation frequencies in a cylindrical fluidized bed of 15 cm i.d. For a freely bubbling bed of glass beads of 450–540 $\mu$m at $u_0/u_{mf} = 2$ and a bed height of 31 cm, the two frequency peaks determined from the power spectrum (figure 3a of the paper) were found to be 2.33 Hz (dominant frequency) and 3.53 Hz (side frequency). Although the

dominant fluctuation frequency of the bubbling bed was reportedly not repeatable in the experiments, an average value of 2.3 Hz can be evaluated from their data (figure 6 in the paper). Using the standing surface wave model, we obtained $f_{1/2} = 2.47$ Hz and $f_1 = 3.56$ Hz. Thus, their data agree well with the antisymmetric and axisymmetric modes of the solids sloshing motion. When other particles (sand of 850–1000 $\mu$m and alumina of 3000 $\mu$m) were used, the bed was observed in a slugging state and slugging frequencies in the range 1–1.5 Hz were obtained, which are distinctly lower than the frequencies of the bubbling bed.

Rockey *et al.* (1989) measured the fluctuation frequencies of 3.18 mm diameter Nylon particles in a cylindrical bed of 30.8 cm i.d. and 46 cm high. The power spectra at four velocities were presented. At $u_0/u_{mf} = 1.1$, the bed was observed to be slugging and the spectrum showed a dominant frequency at 0.9 Hz. Two small peaks at frequencies of 1.7 and 2.6 Hz were also identifiable from the spectrum. At $u_0/u_{mf} = 2.6$ and 5, a freely bubbling bed was observed and the dominant frequency was about 1.65 Hz. The spectrum for $u_0/u_{mf} = 2.6$ also showed a secondary frequency at about 3 Hz. At $u_0/u_{mf} = 8.5$, the bed material was elutriated continuously from the vessel and the pressure fluctuations diminished. Again, using the standing surface wave model, we found $f_{1/2} = 1.72$ Hz and $f_1 = 2.49$ Hz. Thus, a good agreement is also obtained.

While the present investigation is concerned mainly with sloshing motion, the following comments on slugging are appropriate. There are two kinds of slugging motions, one is associated with plane voids (square-nosed plug) occupying the entire cross section of the bed column, and the other is associated with large (round capped) bubbles of sizes comparble to the bed diameter. The first kind of slugging may exist when $u_0$ is just larger than $u_{mf}$ and is increasing. An example is the 15 cm i.d. bed of Noordergraaf *et al.* (1987) with sand particles of 850–1000 $\mu$m and alumina of 3000 $\mu$m. Similar slugging was also observed in our 190 mm i.d. bed with glass spheres of mean diameter of 2.6 mm. The height of the plane void was found to vary from a few millimeters to a few centimeters, depending on the gas velocity. However, for large-diameter fluidized beds, the voids may break down into bubbles, as reported by Rockey *et al.* (1989) in their 30.8 cm i.d. bed with 3.18 mm Nylon spheres. All of these particles belong to the Geldart group D classification. Therefore, the mechanism responsible for this kind of slugging may be related to the particle properties. The definitive answer has to come from further study. The second kind of slugging appears in deep beds (e.g. $H/D > 2$) with $u_0$ being such that complete bubble coalescence takes place. Such was the case for the experiments of Baeyens & Geldart (1974). The data reported by Noordergraaf *et al.* (1987) for the first kind of slugging and by Baeyens & Geldart (1974) for the second kind of slugging seem to suggest that the fluctuation frequency of both kinds of slugging depends only on the bed diameter and height (different dependence as given by [2] and [4], respectively). It is also interesting to note that these slugging frequencies are distinctively lower than the sloshing frequency for the same bed diameter.

## 6. CONCLUDING REMARKS

From the foregoing discussion it can be concluded that sloshing is the dominant mechanism of solids global fluctuations in bubbling fluidized beds, and the sloshing frequency can be reasonably well predicted by the standing surface wave model. It is also seen that information on the dominant frequencies alone is insufficient to identify the mechanisms of solids fluctuations, especially when sloshing and slugging are competing mechanisms in fluidized beds of intermediate depth. The slugging models of Verloop & Heertjes (1974) and of Baeyens & Geldart (1974) are not applicable to bubbling beds of shallow and intermediate depth. For beds of the same geometry, the slugging frequency is always lower than the sloshing frequency since slugging is characterized by the completion of bubble coalescence and therefore is associated with large bubbles (or slugs). Similarly, antisymmetric sloshing has a lower frequency than axisymmetric sloshing because the former is associated with larger bubbles, as illustrated in figure 7. The standing wave model is expected to find applications for large commercial fluidized beds where bubbling is the dominant feature.

*Acknowledgement*—The work was supported by Department of Energy through Grant DE-FG22-85PC80511, administered by University Coal Research Program, Pittsburgh Energy Technology Center.

## REFERENCES


AI, Y. H. 1991 Solids velocity and pressure fluctuation measurements in air fluidized beds. M.S. Thesis, Univ. of Illinois, Urbana, IL.

ANDERSON, T. B. & JACKSON, R. 1968 Fluid mechanical description of fluidized beds—stability of state of uniform fluidization. *Ind. Engng Chem. Fundam.* **7,** 12–21.

ANDERSON, T. B. & JACKSON, R. 1969 A fluid mechanical description of fluidized beds—comparison of theory and experiment. *Ind. Engng Chem. Fundam.* **8,** 137–144.

BAEYENS, J. & GELDART, D. 1974 An investigation into slugging fluidized beds. *Chem. Engng Sci.* **29,** 255–265.

BAIRD, M. H. I. & KLEIN, A. J. 1973 Spontaneous oscillation of a gas-fluidized bed. *Chem. Engng Sci.* **28,** 1039–1048.

BENDAT, J. S. & PIERSOL, A. G. 1986 *Random Data: Analysis and Measurement Procedure*, 2nd edn. Wiley, New York.

BOTTERILL, J. S. M., GEORGE, J. S. & BESFORD, H. 1966 Bubble chains in gas fluidized beds. *Chem. Engng Prog. Symp. Ser.* **62,** 7–14.

BROADHURST, T. E. & BECKER, H. A. 1976 Measurement and spectral analysis of pressure fluctuations in slugging beds. In *Fluidization Technology*, Vol. 1 (Edited by KEAIRNS, D. L.), pp. 63–85. McGraw–Hill, New York.

CANADA, G. S., MCLAUGHLIN, M. H. & STAUB, F. W. 1978 Flow regimes and void fraction distribution in gas fluidization of large particles in beds without tube banks. *AIChE. Symp. Ser.* **74,** 14–26.

DAVIDSON, J. F. 1968 Rapporteur's account. Presented at the *Tripartite Chem. Engng Conf., Symp. on Fluidization*, Montreal, Canada.

DIDWANIA, A. K. & HOMSY, G. M. 1981a Rayleigh–Taylor instabilities in fluidized beds. *Ind. Engng Chem. Fundam.* **20,** 318–323.

DIDWANIA, A. K. & HOMSY, G. M. 1981b Flow regimes and flow transitions in liquid fluidized beds. *Int. J. Multiphase Flow* **7,** 563–580.

EL-KAISSY, M. M. & HOMSY, G. M. 1976 Instability waves and the origin of bubbles in fluidized beds—part 1: experiments. *Int. J. Multiphase Flow* **2,** 379–395.

FAN, L. T., HO, T., HIRAOKA, S. & WALAWENDER, W. P. 1981 Pressure fluctuations in a fluidized bed. *AIChE Jl* **27,** 388–396.

FAN, L. T., HIRAOKA, S. & SHIN, S. H. 1984 Analysis of pressure fluctuations in a gas–solid fluidized bed. *AIChE Jl* **30,** 346–349.

GELDART, D. 1973 Types of gas fluidization. *Powder Technol.* **7,** 285–292.

GOOSSENS, W. R. A. 1976 Dynamic characteristics of a gas fluidized bed. In *Fluidization Technology*, Vol. 1 (Edited by KEAIRNS, D. L.), pp. 87–93. McGraw–Hill, New York.

HIBY, J. W. 1967 Periodic phenomena connected with gas–solid fluidization. In *Proceedings of the International Symposium on Fluidization*, pp. 99–112. Netherland Univ. Press, Amsterdam.

HIRAOKA, S., SHIN, S. H., FAN, L. T. & KIM, K. C. 1984 Pressure fluctuations in a gas–solid fluidized bed—effect of external noise and bubble residence time distribution. *Powder Technol.* **38,** 125–143.

HOMSY, G. M., EL-KAISSY, M. M. & DIDWANIA, A. 1980 Instability waves and the origin of bubbles in fluidized beds—II: comparison with theory. *Int. J. Multiphase Flow* **6,** 305–318.

JACKSON, R. 1963 The mechanics of fluidized beds: part I. The stability of the state of uniform fluidization. *Trans. Inst. Chem. Engrs* **41,** 13–21.

JONES, B. R. E. & PYLE, D. L. 1971 On stability, dynamics, and bubbling in fluidized beds. *AIChE Symp. Ser.* **67,** 1–10.

KATO, K. & WEN, C. Y. 1969 Bubble assemblage model for fluidized bed catalytic reactors. *Chem. Engng Sci.* **24,** 1351–1369.

KUNII, D., YOSHIDA, K. & HIRAKI, I. 1967 The behavior of freely bubbling fluidized beds. In *Proceedings of the International Symposium on Fluidization*, pp. 243–256. Netherland Univ. Press, Amsterdam.

LEMEHAUTE, B. 1976 *An Introduction to Hydrodynamics and Water Waves*. Springer-Verlag, New York.

LILJEGREN, J. C. 1983 Effects of immersed rod bundles on gross solids circulation in a gas fluidized bed. M.S. Thesis, Univ. of Illinois, Urbana, IL.

LIN, J. S. 1981 Particle-tracking studies for solids motion in a gas fluidized bed. Ph.D. Thesis, Univ. of Illinois, Urbana, IL.

LIN, J. S., CHEN, M. M. & CHAO, B. T. 1985 A novel radioactive particle tracking facility for measurement of solids motion in gas fluidized beds. *AIChE Jl* **31,** 465–473.

LIRAG, R. C. & LITTMAN, H. 1971 Statistical study of the pressure fluctuations in a fluidized bed. *AIChE Symp. Ser.* **67,** 11–22.

MOSLEMIAN, D. 1987 Study of solids motion, mixing, and heat transfer in gas fluidized beds. Ph.D. Thesis, Univ. of Illinois, Urbana, IL.

NOORDERGRAAF, I. W., VAN DIJK, A. & VAN DEN BLEEK, C. M. 1987 Fluidization and slugging in large-particle systems. *Powder Technol.* **52,** 59–68.

ROCKEY, J. M., MEI, J. S., NAKAISHI, C. V. & ROBEY, E. H. 1989 Flow regime characterization of fossil fuel fluidized beds. In *Proceedings of the 1989 International Conference on Fluidized Bed Combustion*, Vol. 1 (Edited by MANAKER, A. M.), pp. 249–258. San Francisco, CA.

RUCKENSTEIN, E. & TZECULESCU, M. 1967 On the hydrodynamics of the fluidized bed. In *Proceedings of the International Symposium on Fluidization*, pp. 180–188. Netherland Univ. Press, Amsterdam.

SVOBODA, K., CERMAK, J., HARTMAN, M., DRAHOS, J. & SELUCKY, K. 1983 Pressure fluctuations in gas-fluidized beds at elevated temperatures. *Ind. Engng Chem. Process Des. Dev.* **22,** 514–520.

SVOBODA, K., CERMAK, J., HARTMAN, M., DRAHOS, J. & SELUCKY, K. 1984 Influence of particle size on the pressure fluctuations and slugging in a fluidized bed. *AIChE Jl* **30,** 513–517.

TAMARIN, A. I. 1964 The origin of self-excited oscillation in fluidized beds. *Int. Chem. Engng* **4,** 50–54.

VERLOOP, J. & HEERTJES, P. M. 1974 Periodic pressure fluctuations in fluidized beds. *Chem. Engng Sci.* **29,** 1035–1042.

WONG, H. W. & BAIRD, M. H. I. 1971 Fluidization in a pulsed gas flow. *Chem. Engng J.* **2,** 104–113.